IEEE Access
Multidisciplinary | Rapid Review | Open Access Journal

Received December 29, 2018, accepted January 4, 2019, date of publication January 11, 2019, date of current version February 4, 2019.

Digital Object Identifier 10.1109/ACCESS.2019.2892121

A Duty Ratio Control Strategy to Reduce Both Torque and Flux Ripples of DTC for Permanent Magnet Synchronous Machines

ZHENG ZHANG AND XINGHUA LIU
School of Mechanical Engineering, Beijing Institute of Technology, Beijing 100081, China
Corresponding author: Zheng Zhang (zhz_bit@163.com)

ABSTRACT This paper proposes a novel duty ratio modulated direct torque control (DDTC) for permanent magnet synchronous motor drive system to achieve high steady performance and reducing ripples of CDTC, especially the ripple of stator flux, which is ignored in the conventional DDTC. The proposed control scheme incorporates the variation rates of current and conventional duty ratio modulation. By introducing the instantaneous variation rates of d-axis current and q-axis current during each sampling cycle into the conventional DDTC, an effective duty ratio modulation method is constituted to determine the time duration of the active voltage vector. Moreover, based on the characteristics of the proposed duty ratio modulation, a weighting coefficient is utilized to improve the performance of the duty ratio modulation. The proposed method can reduce the ripple of torque and stator flux significantly, as well as reduce the ripple of d–q-axis current. The proposed method can achieve a good performance of the steady operation. The simulations and experimental results validate the effectiveness of the proposed schemes.

INDEX TERMS Direct torque control (DTC), permanent magnet synchronous motor (PMSM), ripple reduction, duty ratio.

I. INTRODUCTION

The steady operations of PMSM need to be providing with high-performance control strategies. Field-oriented control (FOC) and direct torque control (DTC) are two well-established control strategies for the PMSM since its introduction several decades ago [1], [2]. Compared to FOC, DTC does not need current regulators and can provide extremely high transient torque control performance with very simple structure [3], [4]. In addition, it minimizes the parameter dependent and reduces the complexity of the algorithms.

For a two-level voltage source inverter system, eight discrete signals, which are outputted by the controller, can directly drive the inverter to generate the optimal voltage vector to compensate the ripples of torque and stator flux. However, the CDTC has two major drawbacks [5], [6]. One is that the switching frequency varies according to the machine angular velocity and the hysteresis bands of torque and stator flux. The other is that large torque and stator flux ripples are generated. For the traditional DTC, only one voltage vector operates over the whole sampling control period, causes high stator flux ripple, torque ripple and significant instability of machine angular velocity. In most cases, using only one voltage vector during one sampling period does not develop the advantage of DTC.

In the past decades, various modified schemes are proposed to deal with the problems of CDTC. A commonly used way is incorporating the space vector modulation (SVM) in CDTC to produce continuous voltage vectors, namely SVM-DTC. SVM can generate an arbitrary voltage vector within its linear range, which overcomes the disadvantage of the switching table in CDTC for only producing eight voltage vectors with fixed magnitude and direction. SVM-DTC can reduce the torque ripple and stator flux ripple with fixed switching frequency. The switching frequency of SVM-DTC is not as high as that of CDTC. The commanded voltage vector can be obtained by various methods, including two resonant controllers [6], the artificial intelligence controller [7]–[10], sliding mode controller [5], etc. By introducing the neural network inverse (NNI) systems into the original BPMSM system, the robustness, static and dynamic performance of the system can be improved [7]. A novel speed observation scheme using artificial neural network (ANN) inverse method is proposed to realize the

speed-sensorless vector drive [9]. Despite the lower torque ripple of SVM-DTC scheme, system complexity and computation burden are more intensive than that of CDTC [11].

Recently, predictive control scheme attracts attention of researchers due to the high performance control for different machines [12]–[16]. DTC combines predictive control and artificial intelligent to improve the dynamic performance and reduce the torque ripple in [14]. According to vector selection and number of applied vectors, predictive control can predict a constant number of the future machine states by using a discrete system model. For the predictive control in [15], the effects of every possible voltage vector are compared with each other and select one voltage vector which can minimize the cost function. A novel fuzzy model predictive direct torque control strategy is proposed in [16], the optimal switching states are determined by the specific operating conditions.

Another sort of popular modified DTC scheme is to introduce the duty ratio of the active vector by dividing one sampling period into several intervals [17]–[22]. The duty ratio can be determined by various optimizations, including an adaptive saturation controller [18], a parameter- independent controller [19], a minimized root mean square (RMS) of torque-ripple controller [20]. The methods differ in the optimization aims and vector numbers. The method in [20] only takes the torque ripple into consideration regardless of the stator flux ripple. The method, despite of reducing the torque ripple, depends too much on the machine parameters and is system complexity. In [21], although it only takes the torque ripple into consideration to determine the duty ratio, a simple and effective method does not rely much on the knowledge of machine parameters. In [22], a novel strategy of DTC is proposed for DFIG, which not only reduces both torque and stator flux ripples, but also normally operates at a low switching frequency. The method is system complexity and has large amount of computation due to the use of two active voltage vectors and one zero voltage vector in each sampling period. The method in [22] reduces the robustness of the control system significantly, because different switching table are applied for dynamic process and steady operation. In [18], a novel strategy applies an adaptive saturation controller into the duty ratio determination. Because the control system does not take the differences of the compensations weight between the torque and stator flux into consideration, it is hard to select optimal active vector and duty ratio for DDTC. In [23], a novel duty ratio modulation strategy by dividing every sector into five small sectors is proposed. A duty ratio control strategy is confirmed on a three-level inverter to reduce torque ripple and improve low-speed performance by the results presented in [24]. Nevertheless, system structure and computational burden are more complicated than that of DDTC on a two-level inverter.

This paper proposes a novel DDTC strategy to improve the performance of both torque and stator flux. The novel DDTC strategy preserves the advantages of simple structure and high torque control performance of CDTC. The detailed expression of d-axis current variations and q-axis current variations are presented to lay the foundation for the duty ratio determination. After that, the overall features of the proposed method are analyzed in detail. Finally, the proposed method is compared with CDTC on the steady-state performances. The simulation and experimental results evaluate the effectiveness of the proposed method on a two-level inverter-fed PMSM drive.

This paper is organized as follows: In Section II, the PMSM model is presented, and in Section III, the principle of the CDDTC is presented. In Section IV, a novel DDTC scheme is proposed, and the proposed duty ratio modulation strategy is analyzed. In Section V, the control strategies of CDTC and proposed DDTC are studied through simulation. Section VI gives detailed experimental results to verify the effectiveness of the proposed scheme. The conclusion is presented in Section VII.

II. MODEL OF PMSM

A. MACHINE EQUATIONS

The model of PMSM is usually formulated in rotor synchronous coordinate, because all the parameters would become constant under steady state condition. Both the stator voltage equation and the stator flux equation of PMSM in d-q reference frame are expressed as follows:

$$U_d = R_s I_d + \frac{d\psi_d}{dt} - \omega\psi_q \tag{1}$$

$$U_q = R_s I_q + \frac{d\psi_q}{dt} + \omega\psi_d \tag{2}$$

$$\psi_d = L_d I_d + \psi_f \tag{3}$$

$$\psi_q = L_q I_q \tag{4}$$

where R_s is the stator resistance; ψ_d and ψ_q are the d-axis and q-axis stator flux, respectively; L_d and L_q are the d-axis and q-axis stator inductance, respectively; ω is electrical rotor speed. ψ_f is permanent magnet flux linkage. U_d, U_q are the d-axis and q-axis stator voltage, respectively; I_d, I_q are the d-axis and q-axis stator current, respectively. The electromagnetic torque is expressed as

$$T_e = \frac{3}{2} p \left(\psi_d I_q - \psi_q I_d\right) \tag{5}$$

Substituting (3) and (4) into (5), the expression of electromagnetic torque can be expressed as

$$T_e = \frac{3}{2} p \left[\psi_f I_q - \left(L_q - L_d\right) I_d I_q\right] \tag{6}$$

where p is the number of pole pairs.

For surface-mounted PMSM, the d-axis and q-axis inductances are equal to synchronous inductance L_s, i.e., $L_d = L_q = L_s$. The electromagnetic torque of surface-mounted PMSM is rewritten as

$$T_e = \frac{3}{2} p \psi_f I_q \tag{7}$$

According to (3) and (4), the d-axis current and the q-axis current can be obtain as

$$I_q = \frac{\psi_q}{L_q} \tag{8}$$

$$I_d = \frac{\psi_d - \psi_f}{L_d} \tag{9}$$

B. EFFECTS OF CURRENT ON TORQUE

The current vector is continuous input variable in surface-mounted PMSM for voltage source inverter, so it is significant to analyze the relationship between the derivation of torque and the derivation of current vector. From (7) and (8), the derivation of the electromagnetic torque with respect to time t is

$$\frac{dT_e}{dt} = \frac{3}{2} p \psi_f \frac{dI_q}{dt} \tag{10}$$

It is seen from (10) that the electromagnetic torque differentiation is proportional to the q-axis current differentiation.

C. EFFECTS OF CURRENT ON THE STATOR FLUX

For surface-mounted PMSM in rotating condition, the stator flux will change whenever the active vectors or the zero vectors are applied. The stator flux is always rotating with the rotor flux. According to (3) and (4), the d-axis stator flux can be controlled effectively by the d-axis current; the q-axis stator flux can be controlled effectively by the q-axis current. The stator flux can be controlled effectively to keep the amplitude and rotational speed of the stator flux. According to (3) – (4), in [21], the derivation of the stator flux with respect to time t is

$$\frac{d\,|\psi_s|}{dt} = \frac{1}{|\psi_s|}\left(\psi_d \frac{d\psi_d}{dt} + \psi_q \frac{d\psi_q}{dt}\right) \tag{11}$$

Substitute (1) and (2) into (11) and omit the tedious derivation process, the derivation of the stator flux is

$$\begin{aligned} |\psi_s| \frac{d\,|\psi_s|}{dt} &= \left(L_d^2 I_d \frac{dI_d}{dt} + L_q^2 I_q \frac{dI_q}{dt} + \psi_f L_d \frac{dI_d}{dt}\right) \\ &= \Delta\psi_{s1} + \Delta\psi_{s2} + \Delta\psi_{s3} \end{aligned} \tag{12}$$

It is seen from (12) that the derivation of the stator flux is composed of three parts. The first part is proportional to the product of d-axis current and its derivation; the second part is proportional to the product of q-axis current and its derivation; the last term is proportional to d-axis current.

From (12), we can get that the stator flux is related to both d-axis current and q-axis current. In other words, it is difficult to independently control the electromagnetic torque and the stator flux in DTC, simultaneously.

For the purpose of reducing torque ripple and stator flux ripple, the variation rates of current are used to determine the duty ratio.

III. PRINCIPLE OF THE CONVENTIONAL DDTC

A. OVERALL CONTROL DIAGRAM

The control diagram of conventional duty ratio control strategy is illustrated in Fig.1. The hardware setup of duty-based

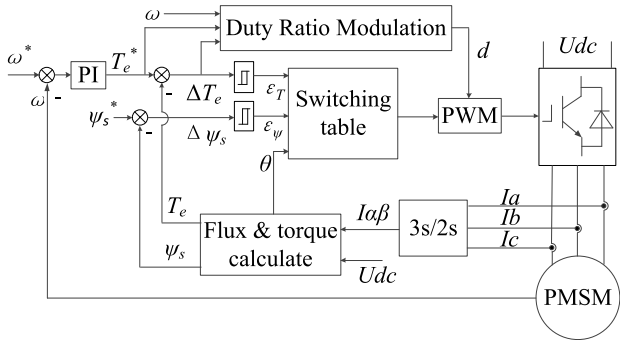

FIGURE 1. Block diagram of conventional DDTC.

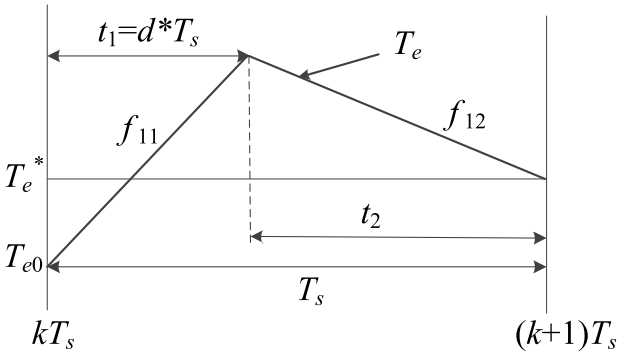

FIGURE 2. Duty ratio determination of conventional DDTC.

DTC is the same of CDTC without any modification. The only difference is that duty ratio modulation is utilized to adjust the action time of the active vector. The conventional DDTC directly uses the errors between the reference values and actual values of torque to determine the duty ratio in [20] and [21].

B. CONVENTIONAL DUTY RATIO DETERMINATION METHOD

For conventional DDTC of voltage source inverter, the voltage vector is an important input variable. The torque error is used to determine the duty ratio in [21].

The duty determination method of conventional DDTC is shown in Fig.2. The principle can be expressed as

$$T_e(k+1) = T_e^* \tag{13}$$

$$t_2 = T_s - t_1 \tag{14}$$

The torque variation rate under active voltage vector is expressed as

$$f_{11} = \left.\frac{dT_e}{dt}\right|_{active} = -\frac{3p}{2L_s}\left(\frac{R_s\psi_{sq}\psi_f}{L_s^2} + \frac{\omega\psi_d\psi_f}{L_s} - \frac{U_q\psi_f}{L_s}\right) \tag{15}$$

When applying zero voltage vectors, the torque variation rate is expressed as

$$f_{12} = \left.\frac{dT_e}{dt}\right|_{zero} = -\frac{3p}{2L_s}\left(\frac{R_s\psi_{sq}\psi_f}{L_s^2} + \frac{\omega\psi_d\psi_f}{L_s}\right) \tag{16}$$

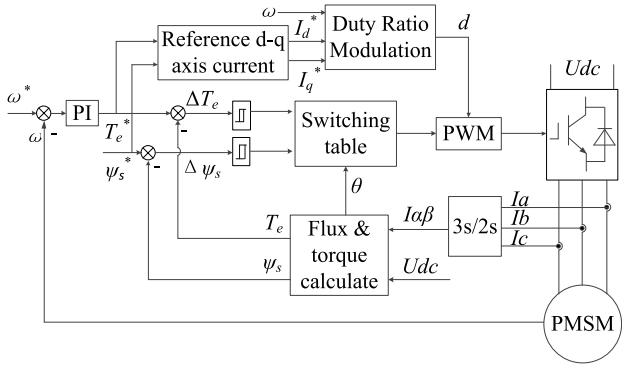

FIGURE 3. Block diagram of proposed DDTC.

According to Fig.2, in [21], in order to solve the time duration of active voltage vector and make the absolute total error of the torque at the end of each control cycle is equal to zero, we assume an equation as

$$E = \left(T_e^e + f_{11}t_1 + f_{12}t_2\right)^2 \tag{17}$$

where $T_e^e = T_e^*$ - T_{e0} is the instantaneous error of torque; T_e^* represents the reference value for torque; T_{e0} indicates the initial torque value; f_{11}, f_{12} represent the torque variation rate of active and zero vectors, respectively. t_1 is the time duration of active voltage vector, T_s is the sampling period.

The equation from (17) can be solved by letting dE/dt=0, the time duration of active voltage vector can be obtained as

$$t_1 = \frac{T_e^e - f_{12}T_s}{f_{11} - f_{12}} \tag{18}$$

IV. PROPOSED DDTC SCHEME

Unlike conventional DDTC, the proposed DDTC utilizes the deviation from the desired values and actual values of the current in two-phase coordinate system. The basic operating principle of proposed DDTC is illustrated in Fig.3, which is similar to that of conventional DDTC. Compared to CDTC, the proposed DDTC has a better performance of reducing both the stator flux ripple and torque ripple. In this paper, the current is used to determine the duty ratio of DDTC.

A. ANALYSIS OF Q-AXIS CURRENT AND D-AXIS CURRENT

The performance of DTC can be analyzed by the variations of stator flux and torque. According to (3)-(5), the torque and stator flux can be controlled by q-axis current and d-axis current. Hence, the variations of q-axis current and d-axis current have an effect on the ripples of torque and stator flux. In this section, the mathematical models of q-axis current and d-axis current under different voltage vectors are investigated, which determine the duty radio of the active voltage vector.

According to (1)-(4), the derivation of q-axis current under active voltage vector is

$$f_{21} = \left.\frac{dI_q}{dt}\right|_{active} = \frac{1}{L_q}\left(U_q - R_sI_q - \omega\psi_f - \omega L_dI_d\right) \tag{19}$$

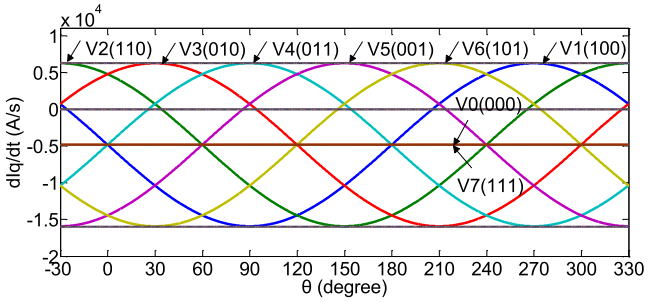

FIGURE 4. The q-axis current slope versus rotor position.

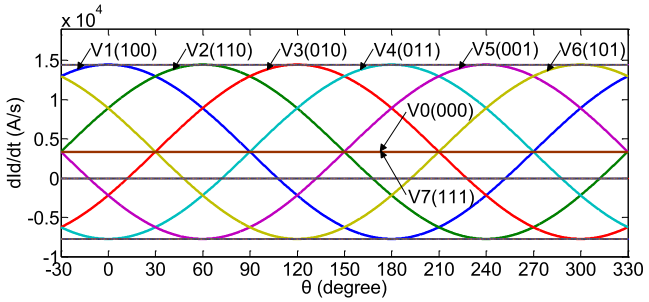

FIGURE 5. The d-axis current slope versus rotor position.

It can be observed that the variation of q-axis current is controlled by the current, instant rotor angular velocity and q-axis stator voltage applied to the machine. Hence, the slope of q-axis current is changing with the operation condition of the machine. Set q-axis stator voltage to zero, and the derivation of q-axis current under zero voltage vector is obtained as

$$f_{22} = \left.\frac{dI_q}{dt}\right|_{zero} = \frac{1}{L_q}\left(-R_sI_q - \omega\psi_f - \omega L_dI_d\right) \tag{20}$$

As we can see from Fig. 4, the signage of di_q/dtin (20) is negative and the decline rate relies upon initial d-q axis current and angular velocity. Hence, the electromagnetic torque decreases under the zero voltage vector. Similarly, the d-axis current differentiation with respect to time t can be obtained from (1)-(4)

$$f_{31} = \left.\frac{dI_d}{dt}\right|_{active} = \frac{1}{L_d}\left(U_d - R_sI_d + \omega L_qI_q\right) \tag{21}$$

It can be observed that the variation of di_d/dt is controlled by the current instant stator current, the rotor angular velocity and d-axis stator voltage decomposed from the stator voltage vector. When d-axis stator voltage is zero, (21) becomes

$$f_{32} = \left.\frac{dI_d}{dt}\right|_{zero} = \frac{1}{L_d}\left(-R_sI_d + \omega L_qI_q\right) \tag{22}$$

According to (22), the variation rate of the d-axis current relies upon the initial q-axis current, the initial d-axis current and angular velocity. As we can see from Fig. 5, the variation rate of the d-axis current does not have an obvious changed under the zero voltage vectors.

TABLE 1. Parameters of drive system.

p	number of pole pairs	4
ψ_f	permanent magnet flux	0.038Wb
R_S	stator resistance	0.901Ω
L_d ,L_q	d-axis and q-axis inductance	6.552mH
ω	rated speed	900r/min
T_N	rated torque	1.5Nm
U_{dc}	DC bus voltage	110V
T_s	sampling period	100μs

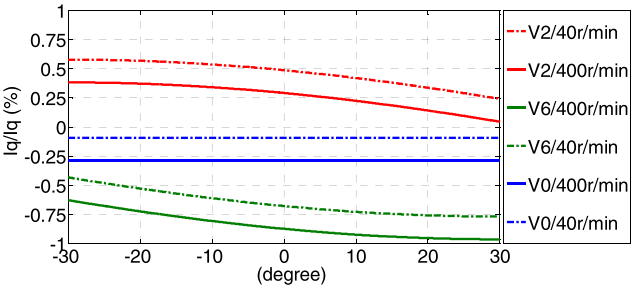

FIGURE 6. The q-axis current variation versus angular location of rotor.

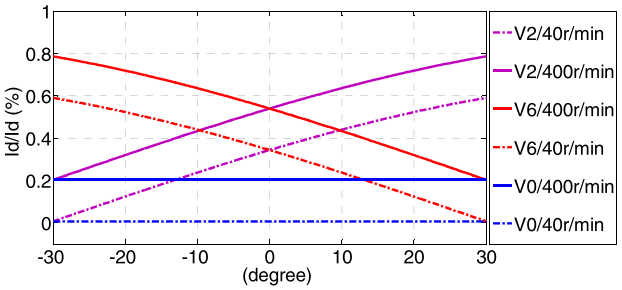

FIGURE 7. The d-axis current variation versus angular location of rotor.

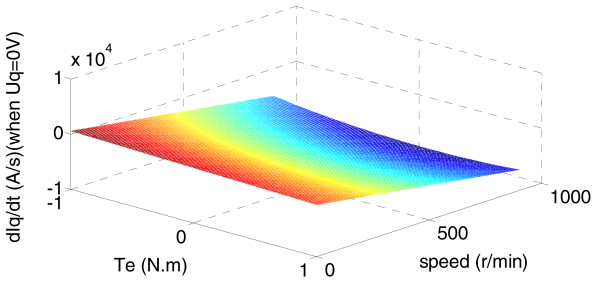

FIGURE 8. The q-axis current variation with different torque and various rotor speed under zero stator voltage vector.

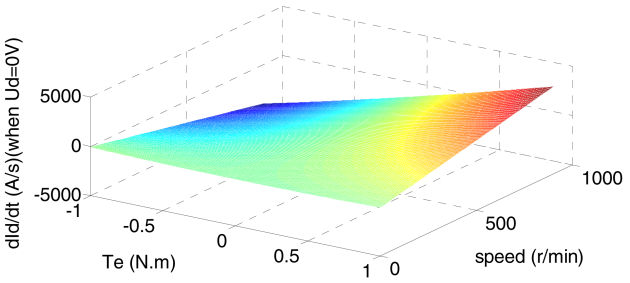

FIGURE 9. The d-axis current variation with different torque and various rotor speed under zero stator voltage vector.

Fig. 4 and Fig. 5 graphically illustrate the variation rates of instantaneous d-q-axis current at varied angular location of flux under eight stator voltage vectors in two-level inverter. The testing surface-mounted PMSM parameters are listed in the Table 1. The machine operates under steady-state at 400 r/min with no load torque. It is obvious that zero voltage vectors have a negative effect on the variation of q-axis current slope. For d-axis current slope, the variation rate is positive under zero voltage vectors. It should be noted that the machine parameters and the rotor angular velocity affect the position of peak points for q-axis current and d-axis current. The values of the peak points for variation rates of both q-axis current and d-axis current are mainly determined by dc bus voltage.

It should be noted that the variation rates of q-axis current and d-axis current are calculated by using the initial current component of q-axis and d-axis current and the rotor angular velocity, regardless of the change of the rotor position during one control period. The calculation of variation rates of both q-axis current and d-axis current will be complicated if the change of angular location of rotor is considered during one control period.

According to (10)-(12), it can be seen that the variation rate of d-axis current does not control the variation rate of torque, while the variation rate of torque is proportional to the variation rate of q-axis current. It is obvious that the variation rates of both d-axis current and q-axis current have a significant effect on the variation rate of stator flux.

In order to investigate the effect of current on different operating condition, the current variation rates are obtained by the computation of (19)-(22) under different angular location of rotor flux and machine angular velocity in Fig.6 and Fig.7. The current variation rate is a percentage of the reference value of d-axis current and q-axis current, respectively. It is shown that the machine angular velocity affects the current variations obviously in Fig.6 and Fig.7. The q-axis current variation rate is smaller than that of low-speed regions, while d-axis current variation rate is larger than that of low-speed regions. The q-axis current variation rate is negative and constant under zero voltage vectors, while the d-axis current variation rate is positive and constant under zero voltage vectors.

It could be found that the torque and rotor speed are related to the variation rates of q-axis current from Fig. 8, when q-axis stator voltage is zero. The variation rates of q-axis current decreases with the increasing of rotor speed significantly. Fig. 9 shows the variation rates of d-axis current is affected by the torque and rotor speed. When the torque is positive, the variation rates of d-axis current increases as the rotor

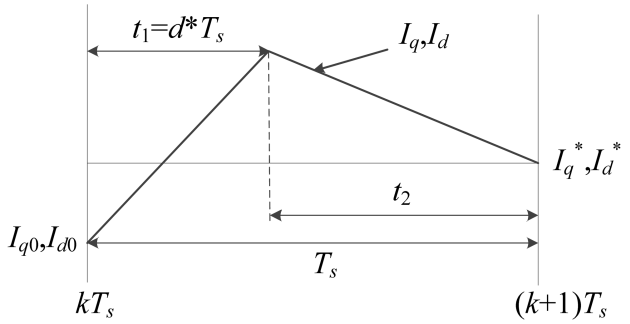

FIGURE 10. Duty ratio determination of proposed DDTC.

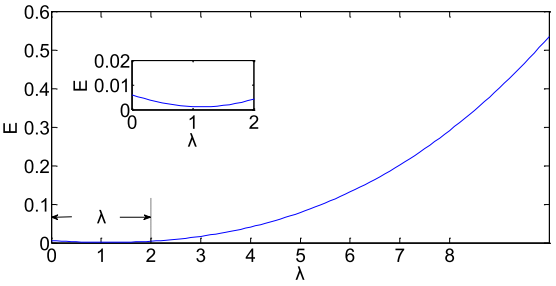

FIGURE 11. The relationship between the corresponding weighting coefficient and the instantaneous minimum error.

speed increase. When the torque is negative, the variation rates of d-axis current decreases as the rotor speed increase.

B. THE NOVEL DUTY RATIO DETERMINATION METHOD

From (19)-(22), it is obvious that the variation rates of d-axis current and q-axis current of the machine can be controlled by adjusting the duration of the selected active voltage vector. Hence, it is possible to reduce both the stator flux ripple and torque ripple by employing the novel duty ratio determination method during the sampling period.

The determination of duty ratio uses final value method to achieve the instantaneous minimum error of the control objective at the end of each control period in [21]. For the proposed DDTC in this paper, the corresponding weighting coefficient λ is introduced to adjust the importance of d-axis current error for determining the duty ratio. When $\lambda = 0$, only the variation of q-axis current is considered to determining the duty ratio, which limit the reduction of the stator flux ripple. While the value of λ increases, the proportion of d-axis current in determining the duty ratio is getting bigger. The value of λ determines reduction of stator flux ripple. In practical implementation, the λ can be equal or greater than zero. The principle of the proposed DDTC can be expressed as

$$I_q(k+1) = I_q^* \tag{23}$$
$$I_d(k+1) = I_d^* \tag{24}$$

For simplification of notations, (25) and (26) are introduced

$$f_2 = f_{21} - f_{22} \tag{25}$$
$$f_3 = f_{31} - f_{32} \tag{26}$$

The final value method is used to achieve the instantaneous minimum error of d-axis current and q-axis current at the end of each control period. According to Fig.10, in order to solve the time duration of active voltage vector and make the absolute total error of the d-q axis current at the end of each control cycle is equal to zero, we assume an equation as

$$E = \lambda\left(I_d^e + f_{31}t_1 + f_{32}t_2\right)^2 + \left(I_q^e + f_{21}t_1 + f_{22}t_2\right)^2 \tag{27}$$

where $I_d^e = I_d^*$- I_{d0} is the instantaneous error of d-axis current; $I_q^e = I_q^* - I_{q0}$ is the instantaneous error of q-axis current; I_d^*, I_q^* represent the reference values for d-axis current and q-axis current, respectively; I_{d0}, I_{q0} indicate the initial d-q axis current values, respectively; f_{31}, f_{32} represent the d-axis current variation rates of active and zero vectors, respectively.

The equation from (27) can be solved by letting dE/dt=0, the time duration of active voltage vector can be obtained as

$$t_1 = \frac{\lambda f_3\left(I_d^e - f_{32}T_s\right) + f_2\left(I_q^e - f_{22}T_s\right)}{\lambda\left(f_3\right)^2 + \left(f_2\right)^2} \tag{28}$$

The corresponding duty ratio d can be solved after obtaining the time duration of active voltage vector t_1. It should be note that d is limited within [0, 1], the constraint equation is expressed as

$$d = \begin{cases} 0 & t_1/T_s < 0 \\ t_1/T_s & 0 \le t_1/T_s \le 1 \\ 1 & t_1/T_s > 1 \end{cases} \tag{29}$$

C. IMPACT OF WEIGHTING COEFFICIENT

The corresponding weighting coefficient λ can adjust the reductions between the q-axis current ripple and the d-axis current ripple. The relationship between the corresponding weighting coefficient λ and the instantaneous minimum error E is shown in Fig. 11. It is obvious that the instantaneous minimum error E can be suitable, when the value of corresponding weighting coefficient λis in the range of 0 to 2. When the value of λ is equal to 1.15, the instantaneous minimum error E obtains the minimum value.

When $\lambda = 0$, only the reduction of q-axis current ripple is considered, and the calculation of the duty ratio d can be simplified. The time duration of active voltage vector t_1 can be rewritten as

$$t_1 = \frac{I_q^e - f_{22}T_s}{f_2} \tag{30}$$

When $\lambda = 1$, the weighting coefficient can balance the reductions between d-axis current ripple and q-axis current ripple. The time duration of active voltage vector t_1 can be expressed as

$$t_1 = \frac{f_3\left(I_d^e - f_{32}T_s\right) + f_2\left(I_q^e - f_{22}T_s\right)}{\left(f_3\right)^2 + \left(f_2\right)^2} \tag{31}$$

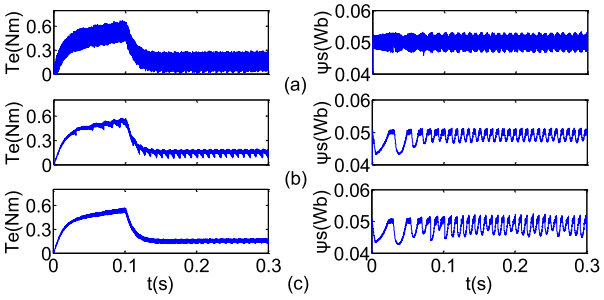

FIGURE 12. Simulation results of torque and stator flux when the motor speed increases from 0 to 300 r/min: (a) CDTC, (b) DDTC ($\lambda = 1$) and (c) DDTC ($\lambda = 0$).

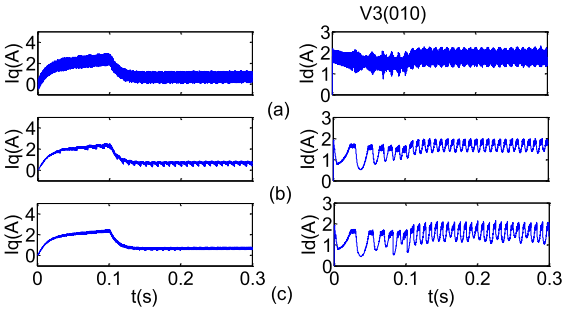

FIGURE 13. Simulation results of d-q axis current when the motor speed increases from 0 to 300 r/min: (a) CDTC, (b) DDTC ($\lambda = 1$) and (c) DDTC ($\lambda = 0$).

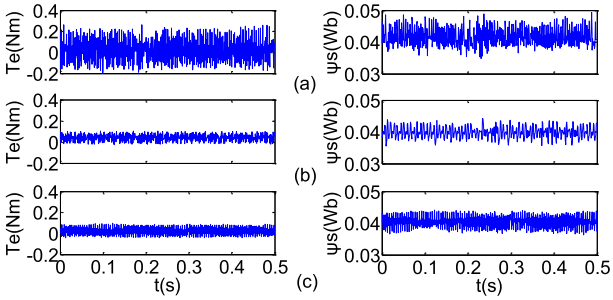

FIGURE 14. Steady state performance of torque and stator flux at rated speed: (a) CDTC, (b) DDTC ($\lambda = 1$) and (c) DDTC ($\lambda = 0$).

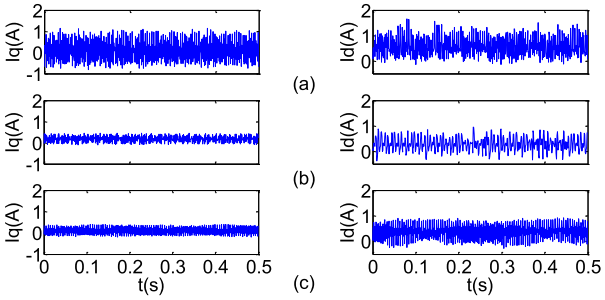

FIGURE 15. Steady state performance of d-q axis current at rated speed: (a) CDTC, (b) DDTC ($\lambda = 1$) and (c) DDTC ($\lambda = 0$).

V. SIMULINK STUDY

In this section, CDTC and the proposed method will be comparatively investigated. The details about two methods are explained in the following. Fig. 12 and Fig. 13 compare the simulation responses for CDTC and the proposed method, respectively. The machine starts-up from standstill to 300r/min with no load. The curves of stator flux and torque are shown in Fig. 12. The curves of d-axis current and q-axis current are shown in Fig. 13.

The steady performance of proposed DDTC is better than that of CDTC in terms of the reductions of torque ripple and stator flux ripple in Fig. 12.

For the proposed method in Fig. 13, it should be noted that the currents in d-q coordinate system is better than that of CDTC during the operation of the machine. Compared to stator flux and d-axis current of DDTC ($\lambda = 0$), the ripples is smaller in DDTC ($\lambda = 1$).

The simulation results indicate that the performance improvement is significant in current, torque and stator flux for proposed DDTC.

VI. EXPERIMENTAL RESULTS

To confirm the effectiveness of the proposed DDTC, a DSP-based PMSM drive system has been set up. The overall control scheme is shown in Fig.3. The experimental setup consists of a dc voltage power supply, a two-level inverter, a DSP digital controller, and a PMSM. The parameters of the PMSM are listed in Table 1. The rotor mechanical speed of PMSM is obtained from a 2500-pulse incremental encoder. A TMS320F28335 DSP control board is employed to implement the real-time algorithm coding using c language, which is also responsible for generating PWM signals and sampling system variables. Two kinds of DTC methods are compared and investigated under steady-state operation conditions, i.e., CDTC and proposed DDTC method. The duty ratio of DDTC is determined by the final value method.

In order to verify the feasibility of the proposed method, experiments are carried out at rated speed without load. The steady-state performances of DTC methods are showed in the follow figures. The curves of electromagnetic torque and stator flux are illustrated in Fig. 14. The curves of d-axis current and q-axis current are showed in Fig. 15.

The steady state performances of torque ripple, stator flux ripple, d-axis current ripple and q-axis current ripple for CDTC, DDTC ($\lambda = 1$) and DDTC ($\lambda = 0$) are showed in Fig. 16 and Fig. 17. The steady state performances of CDTC, DDTC ($\lambda = 1$) and DDTC ($\lambda = 0$) are compared under rated speed conditions without load. The torque ripples of CDTC, DDTC ($\lambda = 1$) and DDTC ($\lambda = 0$) are 0.12, 0.036 and 0.04 N.m, respectively. The average torque of CDTC, DDTC ($\lambda = 1$) and DDTC ($\lambda = 0$) are 0.02, 0.04 and 0.04 N.m, when the machine is run without load at rated speed. The stator flux ripples of CDTC, DDTC ($\lambda = 1$) and DDTC ($\lambda = 0$) are 0.0029, 0.0018 and 0.0021 Wb, respectively. The q-axis current ripples of CDTC, DDTC ($\lambda = 1$) and DDTC ($\lambda = 0$) are 0.55, 0.16 and 0.17 A, respectively. The d-axis current ripples of CDTC, DDTC ($\lambda = 1$) and

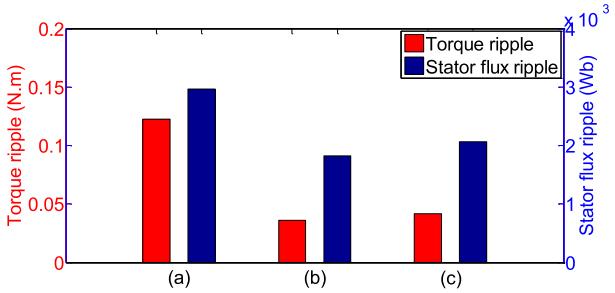

FIGURE 16. Ripples of torque and stator flux at rated speed: (a) CDTC, (b) DDTC ($\lambda = 1$) and (c) DDTC ($\lambda = 0$).

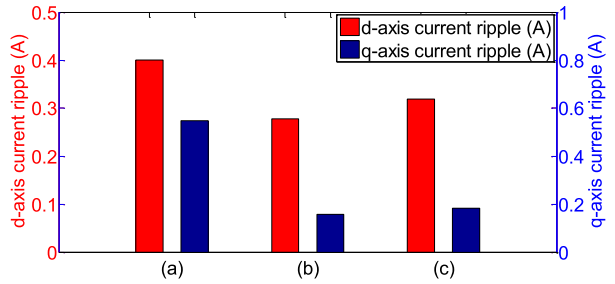

FIGURE 17. Ripples of d-q axis current at rated speed: (a) CDTC, (b) DDTC ($\lambda = 1$) and (c) DDTC ($\lambda = 0$).

DDTC ($\lambda = 0$) are 0.40, 0.28 and 0.31 A, respectively. It is seen that the ripples of torque, stator flux, d-axis current and q-axis current in CDTC are higher than that of DDTC. Thus, DDTC has excellent steady performance. According to these results, it can be seen that proposed DDTC achieves the larger ripple reductions of current, torque and stator flux. Compared to CDTC, the largest ripple reduction of torque is DDTC ($\lambda = 1$), which is 70%, and then followed by DDTC ($\lambda = 0$), with 66.7%; and the ripple reductions of stator flux are 37.8% by DDTC ($\lambda = 1$), 27.6% by DDTC ($\lambda = 0$). Compared to CDTC, the ripple reductions of d-axis current are 30% by DDTC ($\lambda = 1$), and 22.5% by DDTC ($\lambda = 0$); and the ripple reductions of q-axis current are 70.9% by DDTC ($\lambda = 1$), 69.1% by DDTC ($\lambda = 0$).

In addition, the experimental results also indicate that the steady performance of proposed DDCT can be changed by adjusting the weighting coefficient to meet the requirement of practical applications. It can be said that the proposed DDTC scheme shows relatively small ripples of current, torque and stator flux, and the experimental results are similar with the respective simulation results.

VII. CONCLUSION

A very effective method to determining the duty ratio is proposed in this paper, which can significantly reduce ripples of torque and stator flux. The information of machine angular velocity, d-axis current error and q-axis current error are needed in the proposed method, which can be obtained from torque and stator flux. The d-axis current slope and q-axis current slope under different voltage vectors are presented to lay foundation for determining the duty ratio. The effectiveness of the proposed method is verified through simulation and experimental results.

The performance of the proposed method is compared with CDTC by simulations and experiment, and it presents outstanding steady-state performance of torque and stator flux. The comparative study still lacks detailed experiments, and confirming the theoretical analysis and simulations need further investigation.

REFERENCES

[1] Y. Zhou and S. Long, "Sensorless direct torque control for electrically excited synchronous motor based on injecting high-frequency ripple current into rotor winding," *IEEE Trans. Energy Convers.*, vol. 30, no. 1, pp. 246–253, Mar. 2015.

[2] A. K. Jain and V. T. Ranganathan, "Modeling and field oriented control of salient pole wound field synchronous machine in stator flux coordinates," *IEEE Trans. Ind. Electron.*, vol. 58, no. 3, pp. 960–970, Mar. 2011.

[3] A. K. Putri, S. Rick, D. Franck, and K. Hameyer, "Application of sinusoidal field pole in a permanent-magnet synchronous machine to improve the NVH behavior considering the MTPA and MTPV operation area," *IEEE Trans. Ind. Appl.*, vol. 52, no. 3, pp. 2280–2288, May/Jun. 2016.

[4] F. Niu, B. Wang, A. S. Babel, K. Li, and E. G. Strangas, "Comparative evaluation of direct torque control strategies for permanent magnet synchronous machines," *IEEE Trans. Power Electron.*, vol. 31, no. 2, pp. 1408–1424, Feb. 2016.

[5] Y. Zhang, J. Zhu, W. Xu, and Y. Guo, "A simple method to reduce torque ripple in direct torque-controlled permanent-magnet synchronous motor by using vectors with variable amplitude and angle," *IEEE Trans. Ind. Electron.*, vol. 58, no. 7, pp. 2848–2859, Jul. 2011.

[6] A. H. Abosh, Z. Zhu, and Y. Ren, "Reduction of torque and flux ripples in space vector modulation-based direct torque control of asymmetric permanent magnet synchronous machine," *IEEE Trans. Power Electron.*, vol. 32, no. 4, pp. 2976–2986, Apr. 2017.

[7] X. Sun, L. Chen, H. Jiang, Z. Yang, J. Chen, and W. Zhang, "High-performance control for a bearingless permanent-magnet synchronous motor using neural network inverse scheme plus internal model controllers," *IEEE Trans. Ind. Electron.*, vol. 63, no. 6, pp. 3479–3488, Jun. 2016.

[8] X. Sun, Z. Shi, L. Chen, and Z. Yang, "Internal model control for a bearingless permanent magnet synchronous motor based on inverse system method," *IEEE Trans. Energy Convers.*, vol. 31, no. 4, pp. 1539–1548, Dec. 2016.

[9] X. Sun, L. Chen, Z. Yang, and H. Zhu, "Speed-sensorless vector control of a bearingless induction motor with artificial neural network inverse speed observer," *IEEE/ASME Trans. Mechatronics*, vol. 18, no. 4, pp. 1357–1366, Aug. 2013.

[10] X. Sun, B. Su, L. Chen, Z. Yang, X. Xu, and Z. Shi, "Precise control of a four degree-of-freedom permanent magnet biased active magnetic bearing system in a magnetically suspended direct-driven spindle using neural network inverse scheme," *Mech. Syst. Signal Process.*, vol. 88, pp. 36–48, Nov. 2016.

[11] X. Wang, Z. Wang, M. Cheng, and Y. Hu, "Remedial strategies of T-NPC three-level asymmetric six-phase PMSM drives based on SVM-DTC," *IEEE Trans. Ind. Electron.*, vol. 64, no. 9, pp. 6841–6853, Sep. 2017.

[12] M. Habibullah, D. D.-C. Lu, D. Xiao, and M. F. Rahman, "Finite-state predictive torque control of induction motor supplied from a three-level NPC voltage source inverter," *IEEE Trans. Power Electron.*, vol. 32, no. 1, pp. 479–489, Jan. 2017.

[13] R. Morales-Caporal, E. Bonilla-Huerta, M. A. Arjona, and C. Hernandez, "Sensorless predictive DTC of a surface-mounted permanent-magnet synchronous machine based on its magnetic anisotropy," *IEEE Trans. Ind. Electron.*, vol. 60, no. 8, pp. 3016–3024, Feb. 2012.

[14] A. Berzoy, O. Mohammed, and J. Rengifo, "Fuzzy predictive DTC of induction machines with reduced torque ripple and high-performance operation," *IEEE Trans. Power Electron.*, vol. 33, no. 3, pp. 2580–2587, Mar. 2018.

[15] M. Preindl, E. Schaltz, and P. Thogersen, "Switching frequency reduction using model predictive direct current control for high-power voltage source inverters," *IEEE Trans. Ind. Electron.*, vol. 58, no. 7, pp. 2826–2835, Jul. 2011.

[16] J. J. Justo, F. Mwasilu, E.-K. Kim, J. Kim, H. H. Choi, and J. W. Jung, "Fuzzy model predictive direct torque control of IPMSMs for electric vehicle applications," *IEEE-ASME Trans. Mechatronics*, vol. 22, no. 4, pp. 1542–1553, Aug. 2017.
[17] Y. Zhang and J. Zhu, "A novel duty cycle control strategy to reduce both torque and flux ripples for DTC of permanent magnet synchronous motor drives with switching frequency reduction," *IEEE Trans. Power Electron.*, vol. 26, no. 10, pp. 3055–3067, Oct. 2011.
[18] Z. Zhang, C. Wei, W. Qiao, and L. Qu, "Adaptive saturation controller-based direct torque control for permanent-magnet synchronous machines," *IEEE Trans. Power Electron.*, vol. 31, no. 10, pp. 7112–7122, Oct. 2016.
[19] M. A. M. Cheema, J. E. Fletcher, D. Xiao, and M. F. Rahman, "A direct thrust control scheme for linear permanent magnet synchronous motor based on online duty ratio control," *IEEE Trans. Power Electron.*, vol. 31, no. 6, pp. 4416–4428, Jun. 2016.
[20] Y. Ren, Z. Q. Zhu, and J. Liu, "Direct torque control of permanent-magnet synchronous machine drives with a simple duty ratio regulator," *IEEE Trans. Ind. Electron.*, vol. 61, no. 10, pp. 5249–5258, Oct. 2014.
[21] Y. Zhang and J. Zhu, "Direct torque control of permanent magnet synchronous motor with reduced torque ripple and commutation frequency," *IEEE Trans. Power Electron.*, vol. 26, no. 6, pp. 235–248, Jan. 2011.
[22] G. Abad, M. Á. Rodriguez, and J. Poza, "Two-level VSC based predictive direct torque control of the doubly fed induction machine with reduced torque and flux ripples at low constant switching frequency," *IEEE Trans. Power Electron.*, vol. 23, no. 3, pp. 1050–1061, May 2008.
[23] T. Yuan *et al.*, "Duty ratio modulation strategy to minimize torque and flux linkage ripples in IPMSM DTC systems," *IEEE Access*, vol. 5, pp. 14323–14332, 2017.
[24] D. Mohan, X. Zhang, and G. H. B. Foo, "A simple duty cycle control strategy to reduce torque ripples and improve low-speed performance of a three-level inverter fed DTC IPMSM drive," *IEEE Trans. Ind. Electron.*, vol. 64, no. 4, pp. 2709–2721, Apr. 2017.

ZHENG ZHANG received the M.S. degree in electrical engineering from the Anhui Polytechnic University, Wuhu, China, in 2016. He is currently pursuing the Ph.D. degree with the Beijing Institute of Technology, Beijing, China.

His research interests include machine drives and control, intelligent control, and high performance control strategy.

XINGHUA LIU received the Ph.D. degree in power machinery and engineering from the Beijing Institute of Technology, Beijing, China, in 1996.

He is currently an Associate Professor with the Department of Thermal Energy and Dynamics Engineering. His research interests include engine electronic control, intelligent control, and tail gas post-treatment technology.